A parametric computational model of the action potential of pacemaker cells

Weiwei Ai*, Nitish D. Patel, Partha S. Roop, Avinash Malik,
Sidharta Andalam, Eugene Yip, Nathan Allen and Mark L. Trew

***Abstract*—A flexible, efficient and verifiable pacemaker cell model is essential to the design of real-time virtual hearts that can be used for closed-loop validation of cardiac devices. A new parametric model of pacemaker action potential is developed to address this need. The action potential phases are modeled using hybrid automaton (HA) with one piecewise-linear continuous variable. The model can capture rate-dependent dynamics, such as action potential duration (APD) restitution, conduction velocity (CV) restitution, and overdrive suppression by incorporating non-linear update functions. Simulated dynamics of the model compared well with previous models and clinical data. The results show that the parametric model can reproduce the electrophysiological dynamics of a variety of pacemaker cells, such as sinoatrial node (SAN), atrioventricular node (AVN) and the His-Purkinje system (HPS), under varying cardiac conditions. This is an important contribution toward closed-loop validation of cardiac devices using real-time heart models.**

***Index Terms*—Pacemaker cell, hybrid automaton, action potential duration restitution, conduction velocity restitution, overdrive suppression, heart rate variability.**

I. Introduction

CELLS within the cardiac conduction system, including sinoatrial node (SAN), atrioventricular node (AVN) and His-Purkinje system (HPS), can spontaneously initiate action potentials and are referred to as *autorhythmic cells* or *pacemaker cells*. Myocardial cells under some diseased conditions can also possess pacemaking capability [1]. Normally the SAN, the primary intrinsic pacemaker, has the highest spontaneous discharge rate and dominates the heart rhythm. It initiates electrical impulses propagating from atria to ventricles through the AVN and HPS. The subsidiary pacemaker cells in the AVN, HPS and other parts of the heart are usually inhibited by the SAN. Abnormal activation in these subsidiary pacemakers can introduce disturbances in heart activity leading to arrhythmias. The dynamics of pacemaker cells play a crucial role in heart rhythm formation and a corresponding model is, therefore, essential to the development of virtual heart models. However, compared to myocardial cells, electrophysiological data and mathematical models of pacemaker regions, especially in the human heart, are limited [2].

Most biophysical SAN models [3] and AVN models [4] are built around animal data. However, a human SAN model [5] has been developed by combining messenger RNA (mRNA) data with an existing human right atria model [6]. In a similar way, a human AVN model has also been constructed using mRNA data [7]. Stewart and coworkers [8] developed a human Purkinje fiber cell model with detailed ionic mechanisms. The model exhibited overdrive suppression [1], critical to the hierarchy of pacemaker function, but often not a feature of cell models.

Such biophysically-based models provide accurate, realistic and predictive dynamic insights into autorhythmic cell behavior. However, the coupled ordinary differential equations can costly to solve and their solution characteristics may vary between different cell-type models. Fundamentally, the biophysically-based models are not designed for formal verification [9] or real-time emulation [11]. On the other hand, due to the growing use of implantable cardiac devices [14], it has become increasingly important to validate the functionality of these devices under broader physiologically relevant conditions. This necessitates a real-time virtual heart to facilitate the closed-loop validation of the implantable devices [10], [11], [12], [13].

The hybrid automaton (HA) [15] provides a promising formalism to model continuous membrane voltage evolvement and the observed distinct phases of an action potential while retaining computational efficiency and the possibility of formal analysis [9]. Heart models with real-time capacity have been constructed from networks of myocardial nodes [10], [16], [11] using timed automaton (TA) [17] or HA [15]. However, complex pacemaker characteristics were not explicitly modeled. Rather, they have been represented as an arbitrary timer, which was not influenced by external stimuli and could not exhibit realistic dynamics.

Arrhythmias caused by abnormal pacemaking functions are a significant scenario that a cardiac device should respond to. For instance, dysfunction of the SAN remains one of the most common indications for permanent pacemaker implantation [14]. The detection of premature ventricular complexes (PVCs) is crucial for devices to deliver appropriate pacing [18], [19]. Additionally, overdrive pacing from a device may suppress intrinsic pacemaking functions. The time to resumption of the intrinsic rhythm and its dependence on prior pacing rates directly affects subsequent interactions between the device and the heart. Hence, a virtual heart model with the capability

Manuscript received October 7, 2016; revised November XX, 2016; accepted December XX, 2016; This work was partially supported by the CORDIS3D research network (European Union IRSES and the Royal Society of New Zealand). *Asterisk indicates the corresponding author.*

* W. Ai, N. Patel, P. Roop, A. Malik, S. Andalam and N. Allen are with the Department of Electrical and Computer Engineering, University of Auckland, NZ, e-mail: (wai484@aucklanduni.ac.nz).

M. Trew is with Auckland Bioengineering Institute, University of Auckland, NZ.

E. Yip was with the Department of Electrical and Computer Engineering, University of Auckland, NZ. He is currently with the Software Technologies Research Group, University of Bamberg, DE.

exhibiting various pacemaking arrhythmias in real-time is desirable for cardiac devices validation.

In this paper, we develop a computational HA pacemaker cell model with one piecewise continuous variable. The model is able to efficiently describe dynamic electrical behaviors and adaptation to pacing frequency, and compares well to known data. Moreover, the HA model can be parameterized to capture the features of different cardiac pacemaker cells. Pacemaker cell models are combined in a network with myocyte models [11] as the first step toward a comprehensive abstracted heart model with real-time simulation capabilities.

II. Methods

A. SAN and AVN Model

The course of the action potential can be divided into several phases, and the evolvement of each phase is dominated by the movement of various types of ionic currents [20]. The pacemaker cells possess the capability of initiating an action potential without external stimuli, also referred to as *automaticity*. This is due to the slow depolarization in phase 4 (Fig. 1), arising from the "funny"current I_f [1]. Once the threshold potential V_T is reached, an action potential is initiated. Compared to the myocardial action potential (*fast response* type), the action potentials of the pacemaker cells found in SAN and AVN belong to the *slow response* type, where the upstroke (phase 0) is less steep [20].

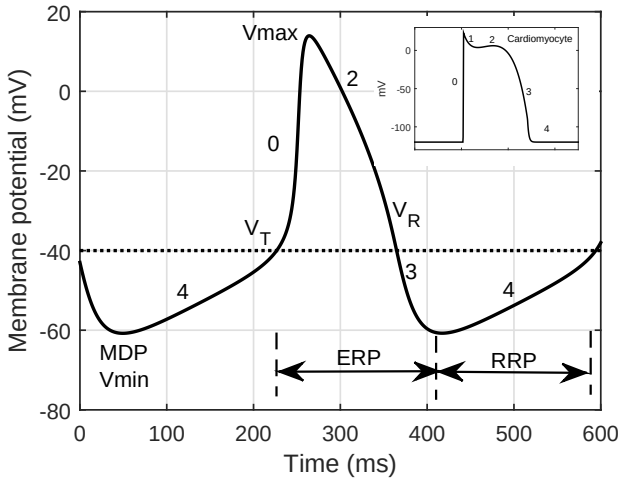

Fig. 1: Schematic action potential of nodal pacemaker cells with the embedded plot of myocardial action potential

During the effective refractory period (ERP), the cell cannot be stimulated again. For the slow response cell, even after complete repolarization (very late in phase 3 or early in phase 4), it may be difficult to be re-excited [20]. Hence, the ERP may expand over phase 0, 2 and 3. The relative refractory period (RRP) extends to phase 4, where a secondary excitation with a small amplitude can be elicited.

The discharge frequency of pacemaker cells may vary by a change in the rate of depolarization in phase 4, the maximal diastolic potential (MDP), or the threshold potential (V_T) (Fig. 1). The rate of rhythm is modulated by both sympathetic and parasympathetic divisions of the autonomic nervous system [1].

If a pacemaker cell is depolarized at a higher frequency than its intrinsic rate, its automaticity may be suppressed, which is known as *overdrive suppression*. The mechanism is mostly due to enhanced activity of the sodium potassium pump resulting in more negative membrane potential. Suppression continues when the overdrive pacing stops and spontaneous depolarization is delayed [1]. The period of quiescence after the cessation of overdrive is referred to as *recovery time*, as shown in Fig. 2.

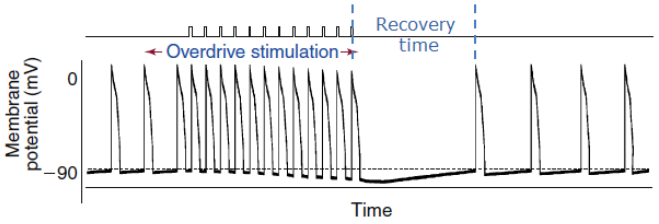

Fig. 2: Overdrive suppression, adapted from [1]

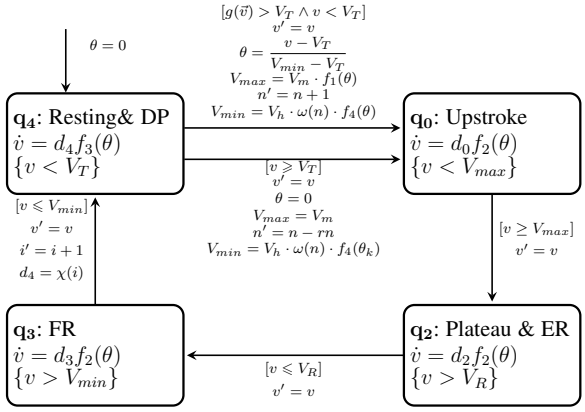

Fig. 3: Pacemaker cell model-Nodal type

We model the action potentials of SAN and AVN with the HA shown in Fig. 3. The locations q_4, q_0, q_2 and q_3 model the dynamics of the action potential in phase 4, 0, 2 and 3 (Fig. 1), respectively. In each location, the membrane potential is defined by a piecewise-continuous variable v.

The parameters d_4, d_0, d_2 and d_3 are the scaling factors of the slope of the action potential. Non-linear functions $f_1(\theta)$, $f_2(\theta)$, $f_3(\theta)$, $f_4(\theta)$ and $\omega(n)$ are used to modify the rate of change of v to capture rate-dependent dynamics. The values of these functions are updated when the transition from q_4 to q_0 occurs.

The pacemaker cell can be excited by its neighboring cells. We calculate the voltage induced at cell k by its n connected neighbors in (1), where D_{ik} denotes the decay factor of the voltage contribution of cell i to cell k:

$$g(\vec{v}) = \sum_{i=1}^{n} D_{ik} \cdot v_i^{out} - v_k \tag{1}$$

By default, the HA always starts in location q_4, where the cell goes through the slow depolarization and the action potential v increases gradually. It stays in q_4 as long as the invariant condition $v < V_T$ is true, where V_T is the threshold potential. Otherwise, it moves to q_0. The last value of v when leaving q_4 is used to set the initial value of v when entering q_0. In location q_0, the cell depolarizes, v increases rapidly and the action potential initiates.

The transition from q_4 to q_0 could be triggered by either of the scenarios:

1) $g(\vec{v}) > V_T \wedge v < V_T$, when the differential voltage between neighboring cells and itself $g(\vec{v})$ is greater than V_T but the membrane potential has not reached the threshold, i.e., the cell is activated by stimuli rather than excited itself;
2) $v \geqslant V_T$, when the membrane potential is greater than V_T, i.e., the cell spontaneously depolarizes.

To express how fast the second excitation occurs, a variable θ that captures the frequency of stimuli is defined by (2). V_{min} represents the maximal diastolic potential (MDP) (Fig. 1) and v is the voltage when the cell is stimulated. For the sake of simplicity, we shift the action potential to be positive and the initial $V_{min} = 0$.

$$\theta = \frac{v - V_T}{V_{min} - V_T} \tag{2}$$

The range of θ is $[0, 1]$ and it is updated when the transition from q_4 to q_0 happens. If the cell is paced faster and activated in the early RRP, the value of θ is closer to 1.

The amplitude and upstroke slope gradually increase as action potentials are stimulated in the late RRP [20]. In our model, the amplitude V_{max} is modified by $f_1(\theta)$ defined by (3) and the slopes in locations q_0, q_2 and q_3 are modified by $f_2(\theta)$ defined by (4). The parameters h and f used in functions (3) and (4) adjust the extent of the frequency dependency.

$$f_1(\theta) = e^{(-h \cdot \theta)} \tag{3}$$

$$f_2(\theta) = e^{(-f \cdot \theta)} \tag{4}$$

When the action potential evolves in q_0, q_2 and q_3, it cannot be excited by any external stimuli, which is the ERP, computed by (5), where V_m is the maximum voltage when the cell itself initiates an action potential and V_R is the voltage where the final repolarization starts.

$$ERP = \frac{V_m \cdot f_1(\theta) - V_T}{d_0 \cdot f_2(\theta)} + \frac{V_m \cdot f_1(\theta) - V_R}{\mid d_2 \mid \cdot f_2(\theta)} + \frac{V_R - V_{min}}{\mid d_3 \mid \cdot f_2(\theta)} \tag{5}$$

Stimulation at high rates can cause lengthy refractory periods (ERP) of AVN leading to conduction blocks [20]. In our model, ERP becomes longer when paced faster as long as the lengthening effect induced by $f_2(\theta)$ and more negative V_{min} exceeds the shortening caused by $f_1(\theta)$.

High-frequency overdrive results in hyperpolarization of resting membrane potential, i.e., more negative MDP and slower depolarization [1]. The study in [21] shows an exponential increase in recovery time with incremental pacing rate. Also, the recovery time depends on the pacing duration. While the longer overdrive duration causes the longer quiescence [1], it will not rise significantly beyond a certain duration [21].

In our model, n is the number of consecutive overdrive stimuli representing the duration of overdrive. We define $\omega(n)$ in (6) to capture the effect of duration. It is incorporated in (7) and (8) to modify d_4 and V_{min}, which are the key parameters affecting the rate of slow depolarization in q_4.

$$\omega(n) = \begin{cases} 0 & \text{if } n < 1 \\ \dfrac{1}{1 + e^{(-h_r \cdot (n - h_s))}} & \text{if } n > 1 \text{ and } n \leq \frac{5}{h_r} + h_s \\ \dfrac{1}{1 + e^{-5}} & \text{if } n > \frac{5}{h_r} + h_s \end{cases} \tag{6}$$

We limit the value of $n \leq \frac{5}{h_r} + h_s$ to avoid numerical overflow when implementing. We also reset the value of $\omega = 0$ when the value of $n < 1$. The parameters h_r and h_s can modulate how fast $\omega(n)$ reaches the plateau $\dfrac{1}{1 + e^{-5}}$.

To capture the impact of pacing rates on recovery time, we use the exponential approximation $f_3(\theta)$ in (7) to modify d_4 in location q_4. The maximal diastolic potential V_{min} is modified by (8) and (9), where V_h is a negative voltage representing the extra hyperpotential.

$$f_3(\theta) = \frac{1}{\omega(n) \cdot m \cdot \theta^s + 1} \tag{7}$$

$$V_{min} = V_h \cdot \omega(n) \cdot f_4(\theta) \tag{8}$$

$$f_4(\theta) = e^{(j \cdot (\theta - 1))} \tag{9}$$

In general, normal SAN has relative resistance to overdrive suppression and subsidiary pacemaker cells are more likely to be suppressed [1]. In our model, the parameter m and V_h are used to control the extent of overdrive suppression. The bigger the values of m and V_h, the longer pause after overdrive pacing. In addition, the parameters s and j can modulate the suppression sensitivity to higher rate stimuli.

After pacing stops, spontaneous depolarization gradually resumes the baseline rate [22]. This is modeled by resetting θ to 0 and reducing the duration effect when the transition from q_4 to q_0 occurs due to $v \geqslant V_T$. This can be expressed as:

$$n' = n - rn \tag{10}$$

The range of parameter r ($r \in \mathbb{R}$) can be $[0, 1]$, which defines the rate of recovery. If $r = 1$, the cell can recover after the first spontaneous beat. When $r = 0$, the cell cannot recover to the baseline rate. The V_{min} (MDP) remains at:

$$V_{min} = V_h \cdot \omega(n) \cdot f_4(\theta_k) \tag{11}$$

where θ_k refers to the value of θ when the last external stimulus activates the cell.

When the action potential reaches V_{max} in q_0, the transition to q_2 is triggered and the membrane potential starts to drop.

The final repolarization phase q_3 is entered and the voltage continues to decrease. Once it reaches the maximal diastolic potential V_{min}, the cell model transitions to q_4 where it goes through slow depolarization again.

The pacemaker cell model as described here can spontaneously initiate an action potential at fixed rates. Inspired by the work [16], we can also capture another important feature, called heart rate variability (HRV) [23], by updating $d_4 = \chi(i)$ on the edge from q_3 to q_4. The value of $\chi(i)$ is defined in (12) and (13). The function $RR(i)$ is the inter-beat (RR) interval series, which is described in the supplementary material.

$$\chi(i) = \frac{V_T - V_{min}}{RR(i) - C} \tag{12}$$

$$C = \frac{V_{max} - V_R}{\mid d_2 \mid} + \frac{V_R - V_{min}}{\mid d_3 \mid} + \frac{V_{max} - V_T}{d_0} \tag{13}$$

By integrating $RR(i)$ to the *pacemaker cell* model, we can capture both intrinsic HRV and the influence of external stimuli. In [16], the rhythm of SAN is independent of the external excitation and therefore cannot capture the dynamics like overdrive suppression.

B. Subsidiary pacemaker cell model

Some subsidiary pacemaker cells like His-Purkinje system (HPS) belong to a fast response category. They behave like cardiomyocytes, but also possess automaticity like the nodal pacemaker cells.

We compose the fast response cardiomyocyte model [11] and the nodal cell model to form the subsidiary pacemaker cell model, as shown in Fig.4. The path model concept is developed in the on-line supplemental material. The length of the path, i.e., the distance between the connected cells, is zero, which means that the pulse propagation between the $Cell_A$ (Nodal cell) and the $Cell_C$ (Cardiomyocyte) does not consume time. The external stimulus V_s is only applied on the $Cell_C$, which produces an action potential v. The $Cell_A$ has no direct interface with the external environment and can only initiate an action potential when it is not suppressed by external stimuli.

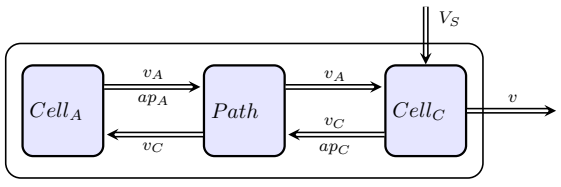

Fig. 4: *Pacemaker cell* model-Subsidiary type

As a result, the pacemaking function of the compositional cell is suppressed when a faster external stimulus is applied. It acts like fast response cardiomyocyte. When the stimuli are absent or the rate is slower than its intrinsic rate, its automaticity emerges due to the pacemaking ability of $Cell_A$. It possesses the same rate-dependent action potential duration (APD) restitution as the fast response cardiomyocyte and suppressed pacemaking dynamics as the slow response nodal cell. As a subsidiary pacemaker cell is more sensitive to overdrive stimuli than nodal cells, we adjust the relevant parameters m, s, V_h, j, h_r, h_s used by (6)-(9) to fit the behavior.

C. Simulation methods

We validated the model by comparing the dynamics with documented quantitative description, clinical study data [21], [24], [25], [26] and simulated dynamics of previous biophysically detailed models [8].

Dynamic behavior was determined by applying various pacing protocols on the proposed model. The cell model was stimulated at various rates (400, 500, 600, 700 ms) and then the ERP was recorded at the ninth beat. We considered ERP rather than APD in this study because the value of ERP can be computed directly and it is the total time spent in locations q_0, q_2 and q_3.

To obtain the overdrive suppression dynamics, overdrive stimuli at the designated rates were applied to the cell model for certain periods and then the recovery time was measured following termination of overdrive. The pacing rates and durations are given in the results.

We intend to use generic models to cover the dynamics of pacemaker cells under various conditions in different regions. The regional differences in electrical properties are accomplished by adjusting the parameters. Table I summarizes the impact of main parameters on the dynamics, where $\uparrow$ and $\downarrow$ denote that positive and negative changes at given θ with an incremental parameter value. The horizontal bar "$-$"denotes no direct impact. In the supplemental material, we present more simulation results to illustrate this.

	Parameters					
Dynamics	h	f	m	s	$\lvert V_h \rvert$	j
V_{max}	$\downarrow$	$-$	$-$	$-$	$-$	$-$
$\lvert V_{min} \rvert$	$-$	$-$	$-$	$-$	$\uparrow$	$\downarrow$
ERP	$\downarrow$	$\uparrow$	$-$	$-$	$\uparrow$	$\downarrow$
Recovery time	$-$	$-$	$\uparrow$	$\downarrow$	$\uparrow$	$\downarrow$

TABLE I: The impact of main parameters

In Section III, we demonstrated the dynamic response of the proposed model by showing the APD restitution of AVN. The key features of overdrive suppression were illustrated on SAN as well as subsidiary ventricular pacemakers by reproducing clinical data and dynamics of previous model. This showed the capability of the parametric model to capture dynamics of a variety of pacemaker cells under varying conditions. Furthermore, a test network of cells along the cardiac conduction system was used to validate the behaviors of the new pacemaker cell models in a virtual heart.

III. Results

A. APD restitution in AVN

Premature stimulation causes lengthening of the ERP in the AVN. This is an important feature to protect the ventricles when atrial impulses arrive at excessive repetition rates [20]. The study in [24] shows that the AVN ERP lengthens 30 ± 39 ms with pacing cycle decrease of 214 ± 63 ms, as shown in Fig. 5A.

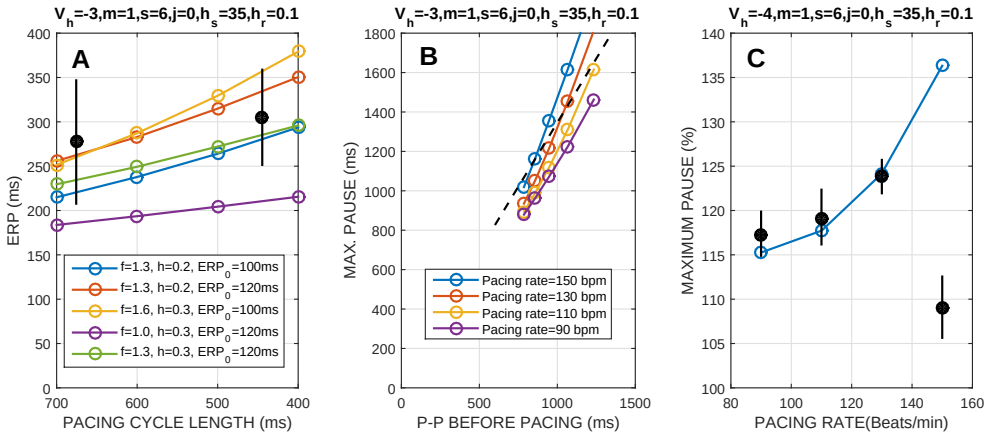

Fig. 5: Dynamic cell response to pacing. A. The rate-dependent response of ERP in an AVN model. Experimental ranges of ERP from [24] are indicated by the mean values and error bars. B. The intrinsic rate of a SAN model compared to the maximum pause in overdrive stimulation. The experimental relationship from [25] is indicated by the dotted line. C. The maximum post overdrive pause as a function of pacing rate in a SAN model. Experimental observations from [25] are shown overlaid on the simulation curve.

In our model, when f increases or h decreases, the ERP lengthens with decreased pacing cycle. We set the intrinsic cycle length at 1500 ms and vary parameters f and h to fit different rate-dependent responses. The ERP is recorded at different pacing cycle lengths. Each circle represents the refractory period measured at that pacing cycle length in Fig. 5A, where ERP_0 denotes the ERP at the intrinsic rate. The result shows a similar trend to published observations [24].

B. Relation between intrinsic sinus rates and the sinus node recovery time (SNRT)

Normally, the SNRT is less than 1500 ms [27] while SNRT tends to be shorter with shorter baseline sinus cycle lengths [25], which is illustrated by the dashed line in Fig. 5B, where P-P denotes the interval between P waves, i.e., intrinsic sinus cycle length, and the maximum pause represents SNRT.

We set the baseline sinus cycle lengths as 786, 858, 947, 1067 and 1234 ms. Then pacing is carried out at different rates (90, 110, 130 and 150 bpm (beats/min)) for 90 seconds. Our model exhibits incremental SNRT with longer baseline cycles, as shown in Fig. 5B.

C. Effect of pacing rates on SAN suppression

The study in [25] shows an increase in the maximum pause of SAN as the pacing rate increases. We pace the model with the intrinsic cycle length of 786 ms. The result in Fig. 5C, where the y-axis is the pause as a percent of the intrinsic cycle length, shows that we can mimic the similar trend except for the drop at 150 Beats/min.

They explain that the drop may be the result of enhanced sympathetic discharge [25]. While d_4 in our model can represent the sympathetic control, we do not link the heart rates to this parameter. In our experiment, the value of d_4 remain the same therefore there is no decrease of SNRT at 150 Beats/min.

D. Effect of pacing rates on subsidiary ventricular pacemaker suppression

An exponential increase in recovery time of subsidiary ventricular pacemaker cells with incremental pacing rates is shown in [21]. We set the interval of intrinsic heart beat 1419 ms to study the effect of pacing rates on the suppression. By adjusting the parameters V_h, m, s, j, we can fit the experimental data in the study [21], [26] as well as the simulation results of the model [8], as shown in Fig. 6.

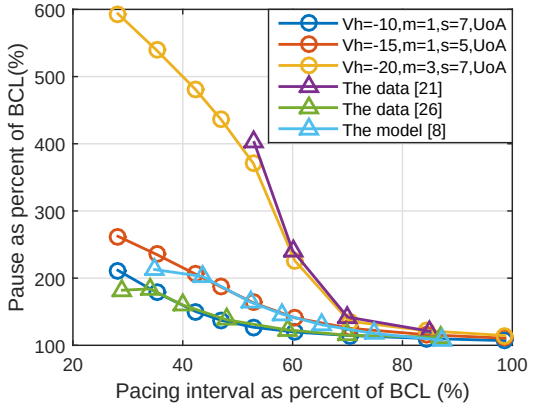

Fig. 6: Effect of pacing rates on recovery time of a Purkinje cell model.

E. Effect of pacing duration on subsidiary ventricular pacemaker suppression

The study [21] shows a biphasic increase in recovery time with incremental pacing duration. Beyond a pacing duration of 60 seconds, ventricular impulse suppression is primarily dependent upon pacing rates. Fig. 7 shows the simulation

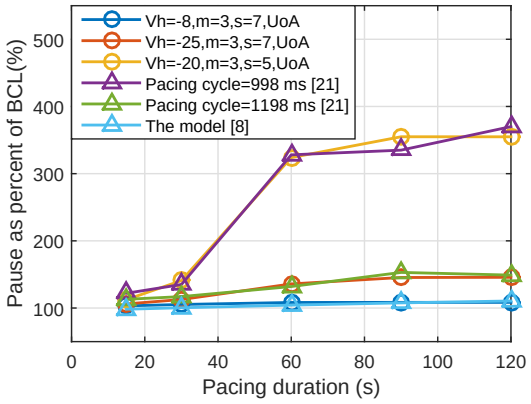

Fig. 7: Effect of pacing durations on recovery time of a Purkinje cell model.

results compared to the study [21] and the simulation results of the model [8], where the cell more depends on duration at higher pacing rates.

F. AVN filtering

We consider a network of cells along the cardiac conduction system to illustrate the behaviors of the new *pacemaker cell* models. The full network is depicted in the on-line supplemental material and Fig. 8A illustrates partial connectivity. Typical action potentials in SAN, atrial subsidiary pacemakers, AVN and ventricular subsidiary pacemakers are shown in Fig. 8C. Fig. 8B shows selected action potentials of atrial muscle (OC), middle of the slow and fast pathway (SP and FP) to AVN , the bundle of His (BH), and the apex of the right ventricle (RVA).

Normally, the SAN inhibits other subsidiary pacemaker cells before they have a chance to depolarize spontaneously to the threshold potential. We block the pathway from the SAN to CT node and enhance the automaticity so that the CT has a chance to overdrive the SAN and other cells. Due to the disturbance of the CT node, the atria present tachycardia.

As the ERP of action potentials along the slow pathway are shorter than the fast pathway, more action potentials pass through. Due to lengthy refractory periods of the AVN and the bundle of His, more action potentials are further filtered and only a fraction of the action potentials reach the ventricles. The frequencies from OC to RVA are 5.3, 4, 3.3, 2.3 and 2.3 Hz, respectively.

When the disturbance of the CT node stops around 15 seconds, there is a pause caused by the *overdrive suppression* effect and the SAN takes longer to resume spontaneous depolarization.

G. Escape ectopic automatic rhythms

Regions of the heart other than the SAN may initiate beats under special circumstances, referred to as *escape ectopic rhythms*. To illustrate this, we enhance the automaticity of the Purkinje fiber so that the RVA has a chance to excite before the impulses from the atria arrive, and the rhythm is often referred to as premature ventricular complex (PVC). In our simulation (Fig. 8B), two consecutive PVCs are observed and followed by a compensatory pause because the ventricles are still in refractory from the PVC and the atrial impulse cannot activate them.

IV. Discussion

In this paper, we have proposed HA models of cardiac pacemaker action potentials and shown that they can capture the key dynamics of the cells. A feature of HA-based models that has been exploited is their support of communication and concurrency between components, which favors compositional design. This has enabled us to model subsidiary pacemaker cells by composing the pacemaker model and a cardiomyocyte model [11] using a path model (Fig. 4). Importantly, the approach enables a single HA formalism to model multiple cell types with just a change of parameterization. This adds computational certainty since the numerical behavior of each cell type will be the same. Furthermore, HA are amenable to formal verification [9], [16] and real-time implementations [12], [28]. This is vital for model-based closed-loop validation of implantable cardiac devices.

Cardiac cells are by nature a hybrid system [9]: transmembrane potentials vary continuously, but distinct phases are present, for which the HA formalism [15] can be employed to describe the hybrid feature. Our choice of piecewise linear approximation of each phase improves computational efficiency. However, to capture the adaptation to pacing frequency requires non-linear functions for which we have used exponential functions. These functions are only updated once in each solution cycle and the increase in computational cost is minimal. Ventricular myocyte HA models have been shown to be amenable to FPGA implementation [28], and we expect similar performance for the models presented in this paper.

Due to the abstracted nature of the HA models, there is no direct link between the model parameters and measurable cellular data. However, we have indicated the effects of parameter movements on key electrophysiological measurements in pacemaker cells that can be robustly measured (Table I). We have shown that most of the available data can be matched using our parameterized HA model [8], [21], [24], [25], [26] and that the parameters can be readily adjusted to capture a variety of pacemaking behaviors with the SAN, AVN and HPS.

In clinical electrophysiological studies [21], [24], [25], [26], external stimuli are usually applied to particular locations in the heart. The observed dynamics are influenced by downstream conductivity, and tissue loading factors that are different to when stimuli are applied to the membrane of a single cell. However, in the absence of other data we have compared the HA cell model behavior to tissue level data. We argue that the resulting parameterizations are sufficiently flexible that when cell level data becomes available the models can still be easily modified to account for this new information.

There are a limited number of data that cannot be replicated by our models (Fig. 5C and Fig. 6), but until there are better biophysical explanations of the functional basis for such behavior this will be a challenge for any model. Apart from

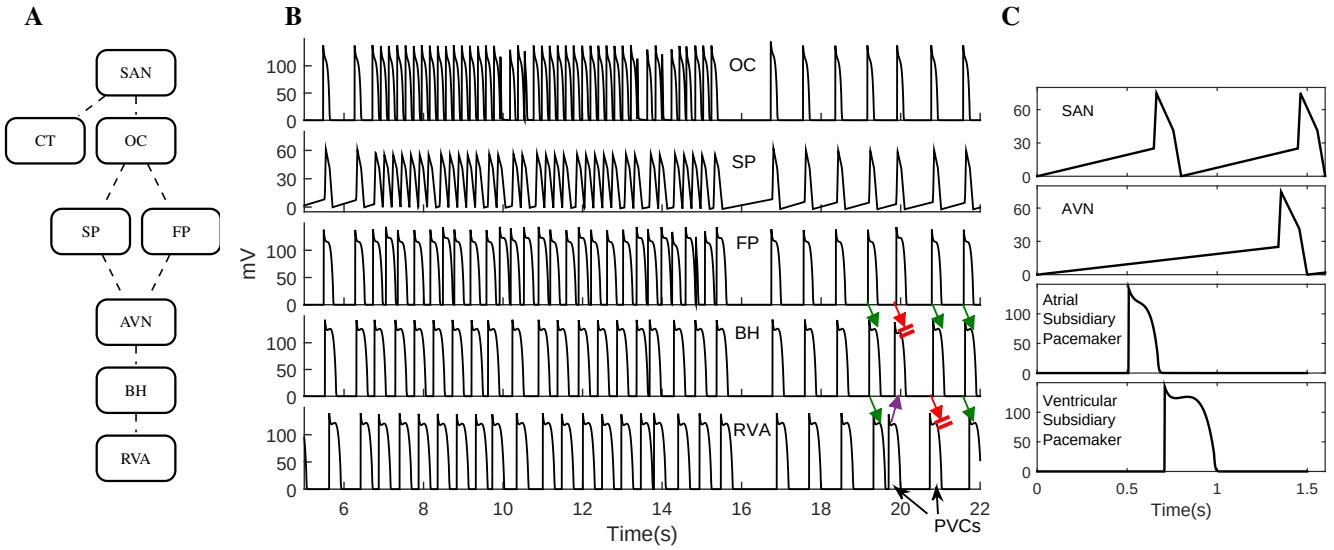

Fig. 8: AVN filtering and PVCs. A. A schematic connectivity between the selected nodes. The connections are dashed as they are only a subset of the network. The full network is given in the supplement, Fig. S3. B. Trains of action potentials from a selection of node, which illustrate AVN filtering and PVCs. The green arrows indicate forward conduction, the purple retrograde conduction from the RVA into the BH and the red arrows indicate possible blocks. C. Typical action potentials.

regional spatial heterogeneity expressed by the SAN, AVN and HPS models, altered electrical dynamics due to cardiac disease conditions can be replicated by altering parameters. Although we have not fully investigated, there is potential for the HA model parameters to be smoothly varied regionally from one cell type to another, accounting for the non-discrete variation of cell types in situ.

In addition to the flexibility and potential real-time implementation, the amiability to formal analysis of HA-based models is vital for the verification of safety-critical devices. The next phase of the study will look at applying formal verification like [16] to the closed-loop network of HA. Model-based testing [29] techniques with a focus on both requirements coverage and structure coverage will also be further investigated.

V. Conclusion

We have developed a new parametric pacemaker cell model to capture electrical restitution, automaticity and overdrive suppression phenomenon. We have compared the simulated dynamics of our model with those of previous models [8], as well as the clinical data [21], [24], [25], [26], and observed that the model is capable of simulating those observed dynamics. Furthermore, our simulation of a conduction system network demonstrates arrhythmias arising from the electrical restitution and abnormal automaticity.

Acknowledgment

The authors express the gratitude to the group of Prof. Henggui Zhang for sharing the C code of Purkinje fiber cell model [8], which was used to validate our model in this paper.

References

[1] Z. F. Issa, J. M. Miller, and D. P. Zipes, "Chapter 3 - electrophysiological mechanisms of cardiac arrhythmias," in *Clinical Arrhythmology and Electrophysiology: A Companion to Braunwald's Heart Disease*, second edition ed., Z. F. I. M. M. P. Zipes, Ed. Philadelphia: W.B. Saunders, 2012, pp. 36 – 61.

[2] M. A. Colman, S. J. Castro, E. A. P. Alday, J. C. Hancox, C. Garratt, and H. Zhang, "Recent progress in multi-scale models of the human atria," *Drug Discovery Today: Disease Models*, vol. 14, pp. 23–32, 2015.

[3] R. Wilders, "Computer modelling of the sinoatrial node," *Medical & biological engineering & computing*, vol. 45, no. 2, pp. 189–207, 2007.

[4] S. Inada, J. Hancox, H. Zhang, and M. Boyett, "One-dimensional mathematical model of the atrioventricular node including atrio-nodal, nodal, and nodal-his cells," *Biophysical journal*, vol. 97, no. 8, pp. 2117–2127, 2009.

[5] N. J. Chandler, I. D. Greener, J. O. Tellez, S. Inada, H. Musa, P. Molenaar, D. DiFrancesco, M. Baruscotti, R. Longhi, R. H. Anderson *et al.*, "Molecular architecture of the human sinus node insights into the function of the cardiac pacemaker," *Circulation*, vol. 119, no. 12, pp. 1562–1575, 2009.

[6] M. Courtemanche, R. J. Ramirez, and S. Nattel, "Ionic mechanisms underlying human atrial action potential properties: insights from a mathematical model," *American Journal of Physiology-Heart and Circulatory Physiology*, vol. 275, no. 1, pp. H301–H321, 1998.

[7] M. A. Colman, "Development of a family of regional cell models," in *Mechanisms of Atrial Arrhythmias*. Springer, 2014, pp. 87–114.

[8] P. Stewart, O. V. Aslanidi, D. Noble, P. J. Noble, M. R. Boyett, and H. Zhang, "Mathematical models of the electrical action potential of purkinje fibre cells," *Philosophical Transactions of the Royal Society of London A: Mathematical, Physical and Engineering Sciences*, vol. 367, no. 1896, pp. 2225–2255, 2009.

[9] P. Ye, E. Entcheva, S. Smolka, and R. Grosu, "Modelling excitable cells using cycle-linear hybrid automata," *Systems Biology, IET*, vol. 2, no. 1, pp. 24–32, 2008.

[10] Z. Jiang, M. Pajic, and R. Mangharam, "Cyber–physical modeling of implantable cardiac medical devices," *Proceedings of the IEEE*, vol. 100, no. 1, pp. 122–137, 2012.

[11] E. Yip, S. Andalam, P. S. Roop, A. Malik, M. Trew, W. Ai, and N. Patel, "Towards the emulation of the cardiac conduction system for pacemaker testing," *CoRR*, vol. abs/1603.05315, 2016. [Online]. Available: http://arxiv.org/abs/1603.05315

[12] N. Allen, S. Andalam, P. Roop, A. Malik, M. Trew, and N. Patel, "Modular code generation for emulating the electrical conduction system

of the human heart," in *2016 Design, Automation & Test in Europe Conference & Exhibition (DATE)*. IEEE, 2016, pp. 648–653.
[13] W. Ai, N. Patel, and P. Roop, "Requirements-centric closed-loop validation of implantable cardiac devices," in *Design, Automation & Test in Europe Conference & Exhibition (DATE)*. IEEE, 2016, pp. 846–849.
[14] H. G. Mond and A. Proclemer, "The 11th world survey of cardiac pacing and implantable cardioverter-defibrillators: Calendar year 2009–a world society of arrhythmia's project," *Pacing and Clinical Electrophysiology*, vol. 34, no. 8, pp. 1013–1027, 2011.
[15] T. A. Henzinger, "The theory of hybrid automata," in *Logic in Computer Science, LICS'96. Proceedings., Eleventh Annual IEEE Symposium on*. IEEE, 1996, pp. 278–292.
[16] T. Chen, M. Diciolla, M. Kwiatkowska, and A. Mereacre, "Quantitative verification of implantable cardiac pacemakers over hybrid heart models," *Information and Computation*, vol. 236, pp. 87–101, 2014.
[17] R. Alur and D. L. Dill, "A theory of timed automata," *Theoretical computer science*, vol. 126, no. 2, pp. 183–235, 1994.
[18] S. S. Barold, R. X. Stroobandt, and B. Herweg, "Automatic mode switching induced by a ventricular bigeminal rhythm: what is the mechanism?" *Pacing and Clinical Electrophysiology*, vol. 35, no. 9, pp. 1158–1161, 2012.
[19] A. El-Damaty, C. Gray, R. Sharma, and J. Sapp, "Atrial pace on pvc algorithm inducing ventricular fibrillation," *Pacing and Clinical Electrophysiology*, vol. 35, no. 6, pp. 749–751, 2012.
[20] A. J. Pappano and W. G. Wier, "2 - excitation: The cardiac action potential," in *Cardiovascular Physiology*, tenth edition ed., A. J. P. G. Wier, Ed. Philadelphia: Elsevier, 2013, pp. 11 – 30.
[21] H. Schmidinger, P. Probst, B. Schneider, H. Weber, and J. Kaliman, "Determinants of subsidiary ventricular pacemaker suppression in man," *Pacing and Clinical Electrophysiology*, vol. 14, no. 5, pp. 833–841, 1991.
[22] Z. Issa, J. Miller, and D. Zipes, "Electrophysiological mechanisms of cardiac arrhythmias: clinical arrhythmology and electrophysiology, a companion to brawnwald's heart disease," *Filadelfia: Saunders*, pp. 1–26, 2009.
[23] G. G. Berntson, J. T. Bigger, D. L. Eckberg, P. Grossman, P. G. Kaufmann, M. Malik, H. N. Nagaraja, S. W. Porges, J. P. Saul, P. H. Stone *et al.*, "Heart rate variability: origins, methods, and interpretive caveats," *Psychophysiology*, vol. 34, no. 6, pp. 623–648, 1997.
[24] I. Wiener, S. Kunkes, D. Rubin, J. Kupersmith, M. Packer, R. Pitchon, and P. Schweitzer, "Effects of sudden change in cycle length on human atrial, atrioventricular nodal and ventricular refractory periods." *Circulation*, vol. 64, no. 2, pp. 245–248, 1981.
[25] W. Mandel, H. Hayakawa, R. Danzig, and H. S. Marcus, "Evaluation of sino-atrial node function in man by overdrive suppression," *Circulation*, vol. 44, no. 1, pp. 59–66, 1971.
[26] S. Rosenheck, C. Bondy, A. T. Weiss, and M. S. Cotsman, "The effect of overdrive pacing rate and duration on ventricular escape rhythms in patients with chronic complete atrioventricular block," *Pacing and Clinical Electrophysiology*, vol. 17, no. 2, pp. 213–221, 1994.
[27] Z. F. Issa, J. M. Miller, and D. P. Zipes, "Chapter 8 - sinus node dysfunction," in *Clinical Arrhythmology and Electrophysiology: A Companion to Braunwald's Heart Disease*, second edition ed., Z. F. I. M. M. P. Zipes, Ed. Philadelphia: W.B. Saunders, 2012, pp. 164 – 174.
[28] S. Andalam, H. Ramanna, A. Malik, P. Roop, N. Patel, and M. L. Trew, "Hybrid automata models of cardiac ventricular electrophysiology for real-time computational applications," in *Engineering in Medicine and Biology Society (EMBC), 2016 IEEE 38th Annual International Conference of the*. IEEE, 2016, pp. 5595–5598.
[29] M. Utting, A. Pretschner, and B. Legeard, "A taxonomy of model-based testing approaches," *Software Testing, Verification and Reliability*, vol. 22, no. 5, pp. 297–312, 2012.

Weiwei Ai received the B.S. degree from Qingdao University, China, in 2003, and the M.E. degree from Beijing University of Technology, China, in 2006. She had been working as a reliability and failure analysis engineer in CEC Huada Electronic Design Co.,Ltd.,from 2006 to 2013. She is currently working towards the Ph.D. degree at the University of Auckland, New Zealand. Her research interests are in verification and validation with a focus on medical devices.

Nitish D. Patel received the B.E. degree from Mangalore University, Karnataka, India, and the Ph.D. degree from the University of Auckland, Auckland, New Zealand. He is currently a Senior Lecturer at the University of Auckland. His research interests include embedded systems, robotics, artificial neural networks, control systems, and hardware implementation of real-time systems for control.

Partha S. Roop received his Ph.D. degree in computer science (software engineering) from the University of New South Wales, Sydney, Australia, in 2001. He is currently an Associate Professor and is the Director of the Computer Systems Engineering Program with the Department of Electrical and Computer Engineering, the University of Auckland, New Zealand. Partha is an associated team member of the SPADES team INRIA, Rhone-Alpes, France, and held a visiting position in CAU Kiel, Germany, and Iowa State University, USA. His research interests include the design and verification of embedded systems. In particular, he is developing techniques for the design of embedded applications in automotive, robotics, and intelligent transportation systems that meet functional-safety standards.

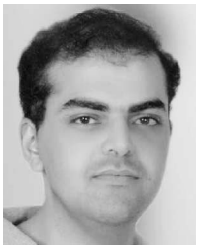

Avinash Malik is a lecturer at the University of Auckland, New Zealand. His main research interest lies in programming languages for multicore and distributed systems and their formal semantics and compilation. He has worked at organizations such as INRIA in France, Trinity College Dublin, IBM research Ireland, and IBM Watson on the design and the compilation of programming languages. He holds B.E. and Ph.D. degrees from the University of Auckland.

Sidharta Andalam received his Ph.D. degree from the University of Auckland, New Zealand, in 2013, where his thesis focused on developing a predictable platform for safety-critical systems. He is currently a research fellow in embedded systems at the University of Auckland, New Zealand. His principle research interest is in the design, implementation, and analysis of safety-critical applications. He has worked at TUM CREATE, Singapore, exploring safety-critical applications in the automotive domain.

Eugene Yip received his B.E. (Hons) and Ph.D. degrees in electrical and computer systems engineering from the University of Auckland, New Zealand. At the start of 2015, he joined the Heart-on-FPGA research group in the Department of Electrical and Computer Engineering, University of Auckland, as a research assistant working on the real-time modeling of cardiac electrical activity. In the middle of 2015, he joined the SWT research group at the University of Bamberg as a research assistant working on synchronous languages. His current research interests include synchronous mixed-criticality systems, parallel programming, static timing analysis, formal methods for organ modeling, and biomedical devices.

Nathan Allen received his B.E. (Hons) degree in Computer Systems Engineering from the University of Auckland, New Zealand. He is currently working towards a Ph.D. degree also at the University of Auckland. His current research interests include the personalised modelling of organs with a further emphasis on real-time execution.

Mark L. Trew attained a Bachelor of Engineering in Engineering Science in 1992 and a Ph.D. Engineering Science in 1999, both from the University of Auckland, New Zealand. He is currently a Senior Research Fellow at the Auckland Bioengineering Institute. Mark constructs computer models and analysis tools for interpreting and understanding detailed images of cardiac tissue and cardiac electrical activity.